

Supplement: Evaluation of the data products used, Tables S1-S2 and Figures S1-S14

Evaluation of the data products used

The AATSR AOD product has been validated with global data (Kolmonen et al., 2016) but as the data set is new we wanted to ensure its suitability for our analysis by comparing it with AOD retrievals done from Multi-angle Imaging SpectroRadiometer (MISR) observations. In practice, we compared monthly averaged L3 AOD products between 2003 and 2011 over the southeastern USA. Both data sets exhibited similar seasonal cycles and trends, and they were very well correlated ($r^2 = 0.92$, Figures S1 and S2). The summertime AOD values in the AATSR data set were larger than the corresponding MISR values but as our analysis is based mainly on anomalies this does not affect the results.

To ensure that the ECHAM-HAMMOZ model could reproduce the observed AOD characteristics at the studied region, it was compared with AATSR observations. The monthly AOD and LST averages from the control simulation (CONTROL) were in reasonable correspondence with the values from the AATSR retrievals for the years 2003-2010 (Figures S3 and S4), even though the satellite data were limited to daytime values only, whereas the model averages included also night-time values. A direct comparison between daytime values only was not possible, because only 24-hour averages were available from the simulation. This simplification does not affect our conclusion because the model simulations with finer temporal resolution (3-hourly) showed that the modelled diurnal variation in AOD was smaller than 0.01. The correlation coefficient for the AOD values was 0.68, the model overestimating the lowest AOD values but underestimating slightly the largest ones. For the LST values, the correlation coefficient was 0.92, the highest temperatures being underestimated in the model due to the inclusion of night-time temperatures in the model averaging. Based on these comparisons, the modelled values agree reasonably well with the observations, which gives us confidence that the model results can be used to illuminate the mechanisms behind the observed phenomena.

Alston et al. (2012) characterized atmospheric aerosols over the southeastern USA using Moderate Resolution Imaging Spectroradiometer (MODIS) and MISR observations. They found that the monthly AOD anomalies between 2001 and 2009 were decreasing by -0.0050 yr^{-1} , -0.0021 yr^{-1} , and -0.0026 yr^{-1} based on MODIS Terra, MISR Terra, and MODIS Aqua, respectively. We did a similar analysis for the years 2003 to 2011 and found corresponding trends: -0.0037 yr^{-1} and -0.0025 yr^{-1} based on AATSR and MISR data, respectively. Attwood et al. (2014) had also studied temporal changes in AOD over the southeastern USA and found that based on the MISR AOD observations AOD had decreased on average by -3.5 \% yr^{-1} between the years 2001 and 2013. We did a similar analysis using both AATSR and MISR AOD data for the years 2003 to 2011. Both instruments produced an identical decrease of -1.7 \% yr^{-1} which is in the same range but slightly smaller than value reported by Attwood et al. (2014). The most likely reason for the difference between the results is the shorter temporal range in our analysis.

Table S1. Satellite product used in the evaluation of the AATSR AOD product.

Product	Usage	Instrument (data depository)	Product type
Aerosol Optical Depth (AOD)	Evaluation of AATSR AOD	MISR (ASDC/NASA)	Level 3, 0.5×0.5 degree, monthly

Table S2. Summer and annual averages of land surface temperature (LST), aerosol optical depth (AOD) and tropospheric NO₂ concentrations (NO2trop) based on AATSR and OMI observations over the southeastern USA.

Year	Summer average			Annual average		
	LST	AOD	NO2trop	LST	AOD	NO2trop
2005	305.53	0.35	2.45E+15	297.83	0.18	3.26E+15
2006	307.04	0.32	2.38E+15	297.71	0.16	3.04E+15
2007	307.61	0.34	2.32E+15	298.88	0.18	3.01E+15
2008	306.57	0.26	2.08E+15	297.92	0.15	2.55E+15
2009	305.89	0.22	1.93E+15	297.37	0.13	2.48E+15
2010	306.90	0.24	2.02E+15	299.93	0.14	2.42E+15
2011	307.95	0.29	2.02E+15	299.77	0.17	2.40E+15

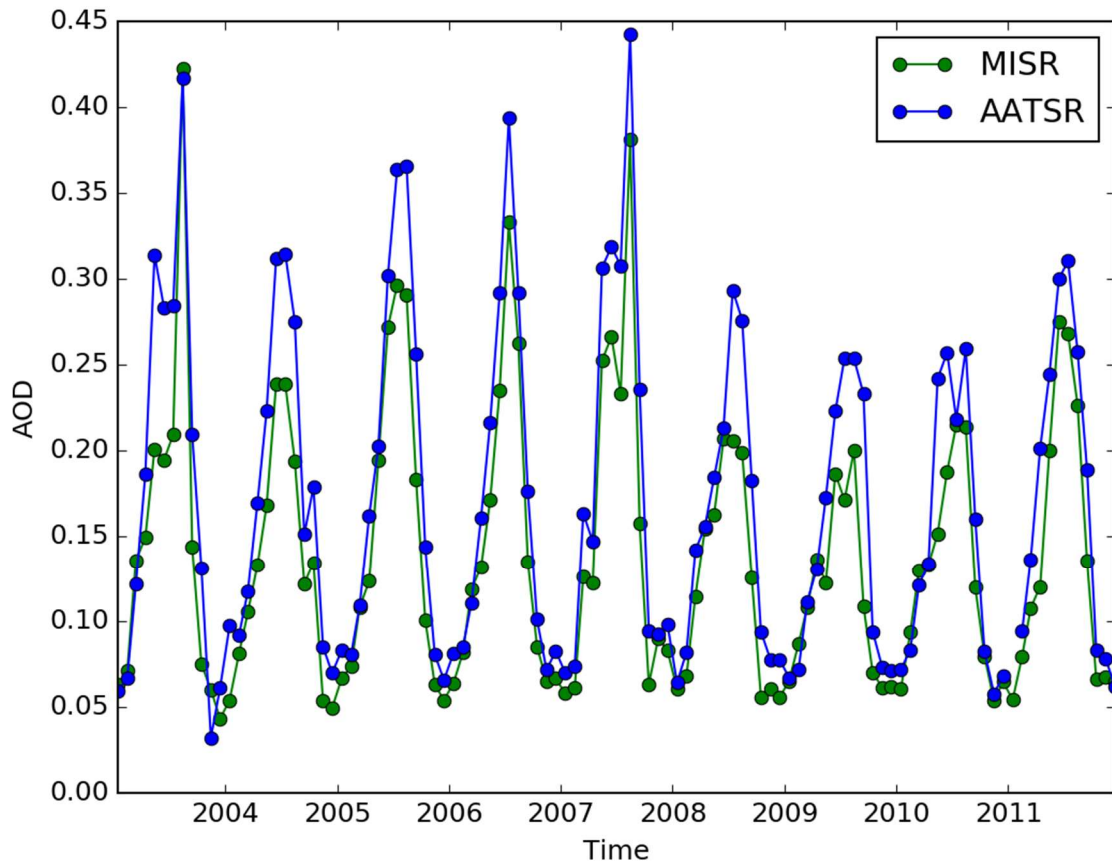


Figure S1. Time series of monthly averaged AOD over the southeastern USA from AATSR and MISR Level 3 products for the years 2003-2011 (108 observations).

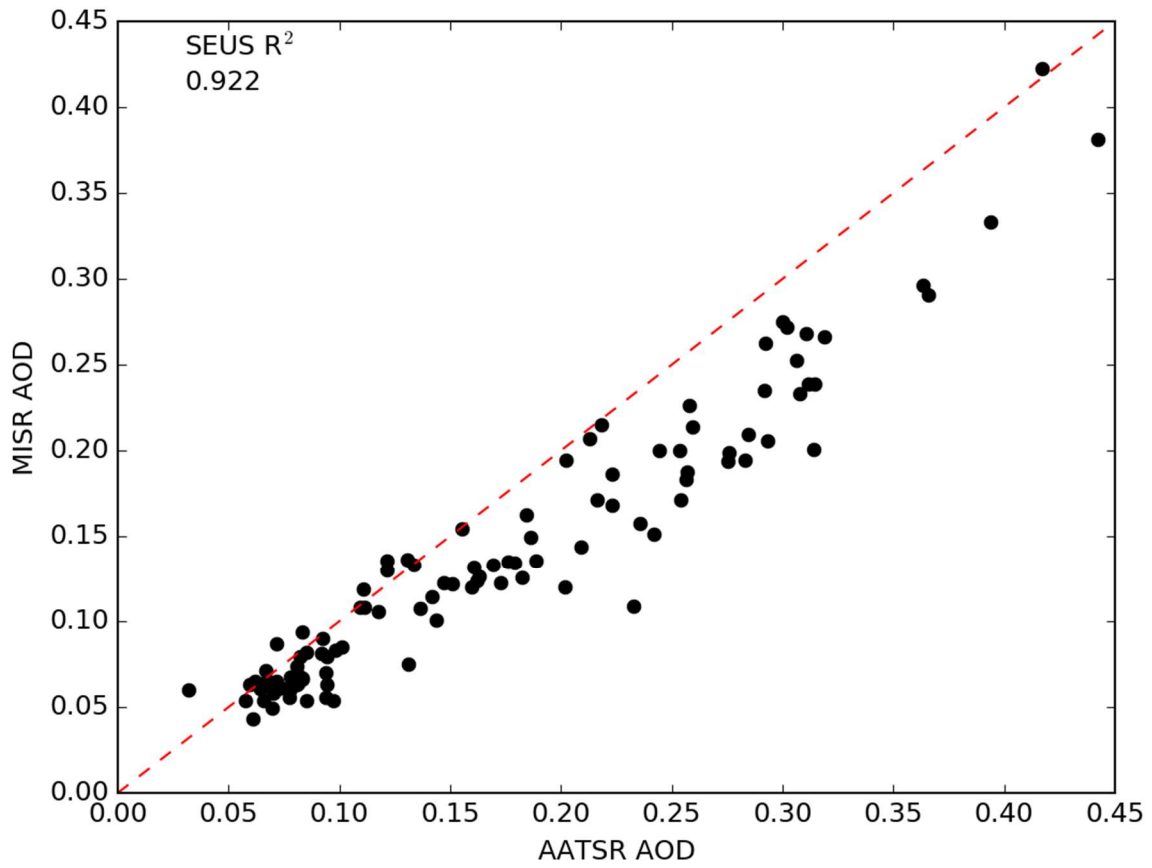


Figure S2. Monthly averaged Level 3 MISR AOD vs. Level 3 AATSR AOD over the southeastern USA for the years 2003-2011 (108 observations). The R^2 refers to the coefficient of determination.

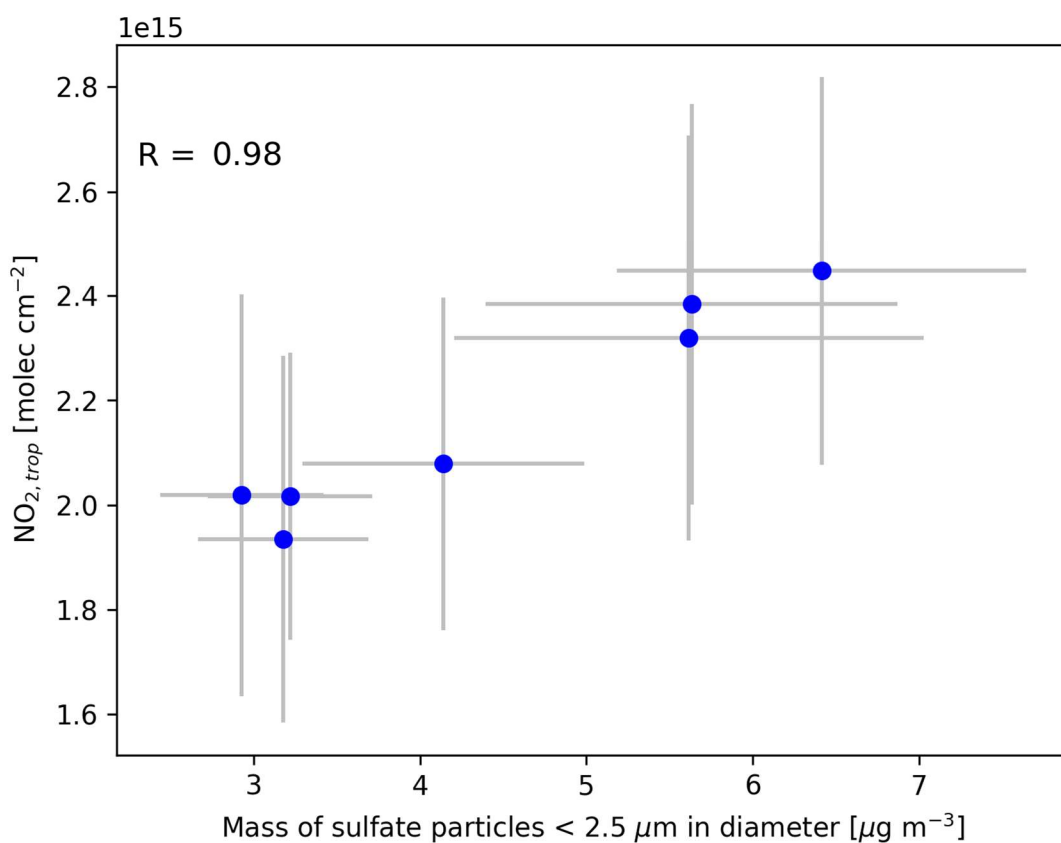


Figure S3. Summertime averaged tropospheric NO₂ column densities vs. sulfate particle mass (diameter below 2.5 μm) in the southeastern USA for the years 2005-2011. The sulfate particle mass averages are calculated from all the available IMPROVE sites within the studied region: Cape Romain, Cohutta, Great Smoky Mountains, Linville Gorge, Mammoth Cave, Mingo, North Birmingham, Okefenokee, Shining Rock Wilderness, Sipsey Wilderness, St. Marks, and Swanquarter. *R* represents the correlation coefficient and the error bars the standard deviation of the values within the summers.

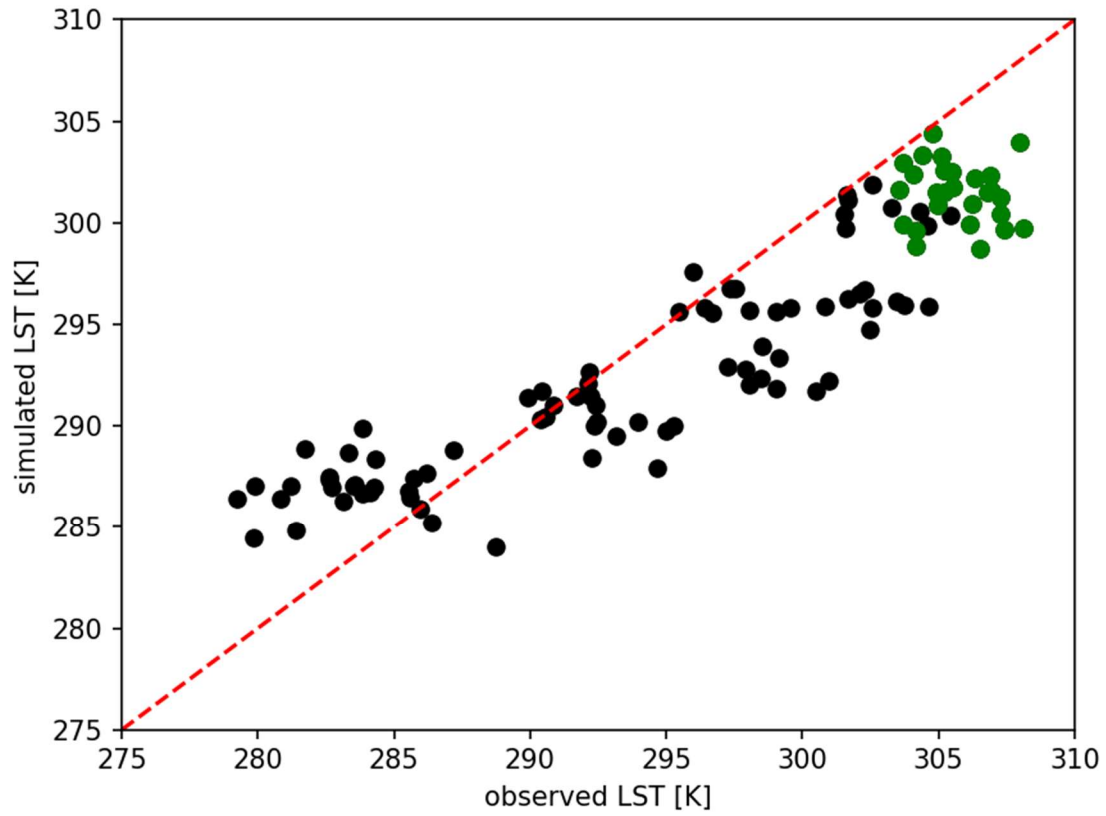


Figure S4. Monthly mean observed LST vs. simulated LST in the southeastern USA for the years 2002–2010 (108 points). Observed LST is based on the L3 AATSR data and simulated on the CONTROL simulation made with ECHAM-HAMMOZ. Summer months (JJA) are shown with green points.

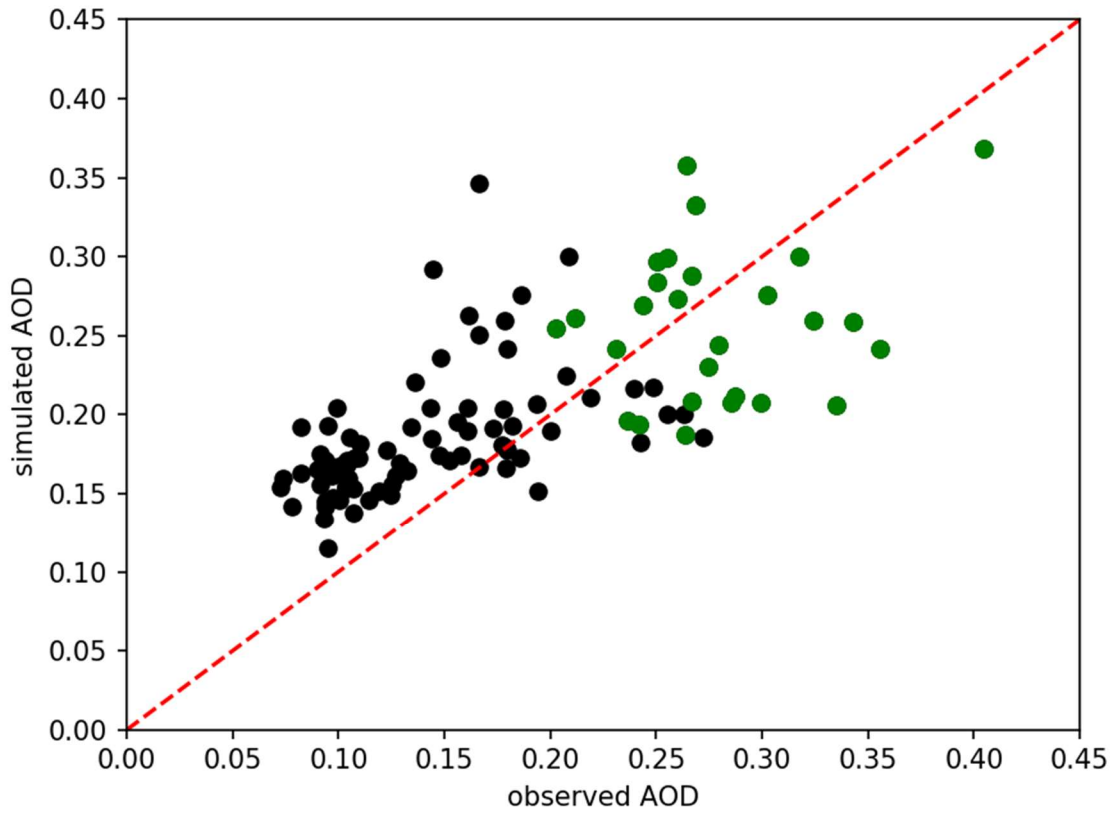


Figure S5. Monthly mean observed AOD vs. simulated AOD over the southeastern USA for the years 2002–2010 (108 points). Observed AOD is based on the L3 AATSR data and simulated on the CONTROL simulation made with ECHAM-HAMMOZ. Summer months (JJA) are shown with green points.

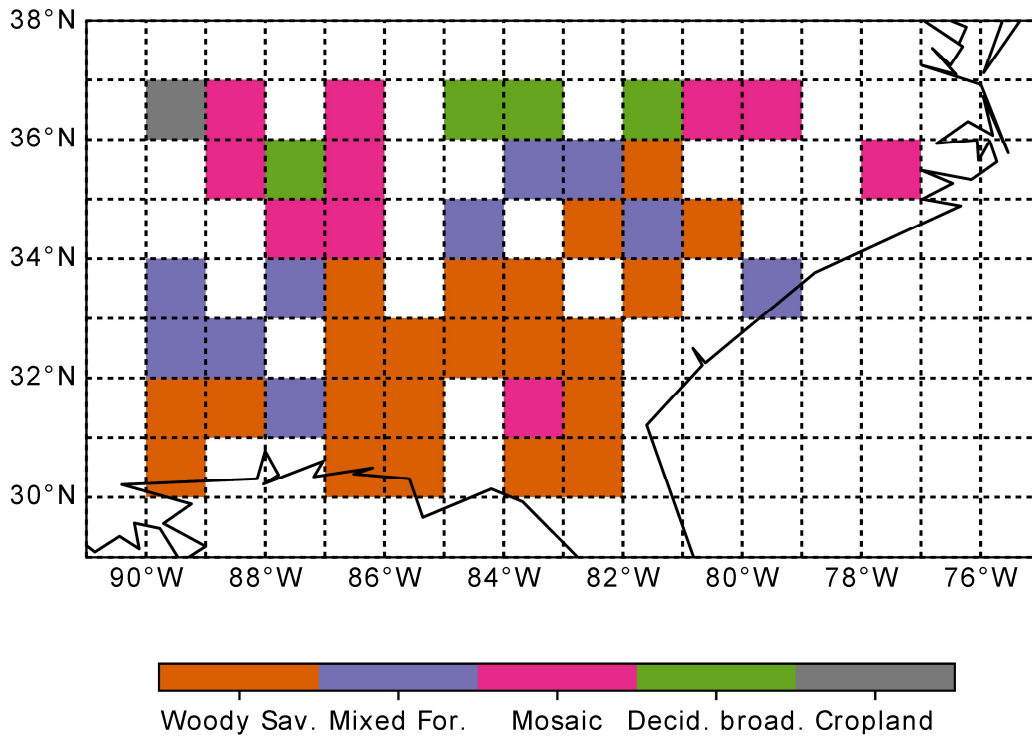


Figure S6. The most common vegetation types in the southeastern USA based on the MODIS MCD12C1 product for the year 2011. IGBP classification was used. A $1^\circ \times 1^\circ$ pixel was considered to be dominated by a certain land cover class if the fraction of that type was 0.5 or larger in the pixel. The five most common land cover classes in 2011 were: woody savannas (22 pixels), mixed forests (13 pixels), cropland/natural mosaic (10 pixels), deciduous broadleaf forests (4 pixels) and cropland (1 pixel)

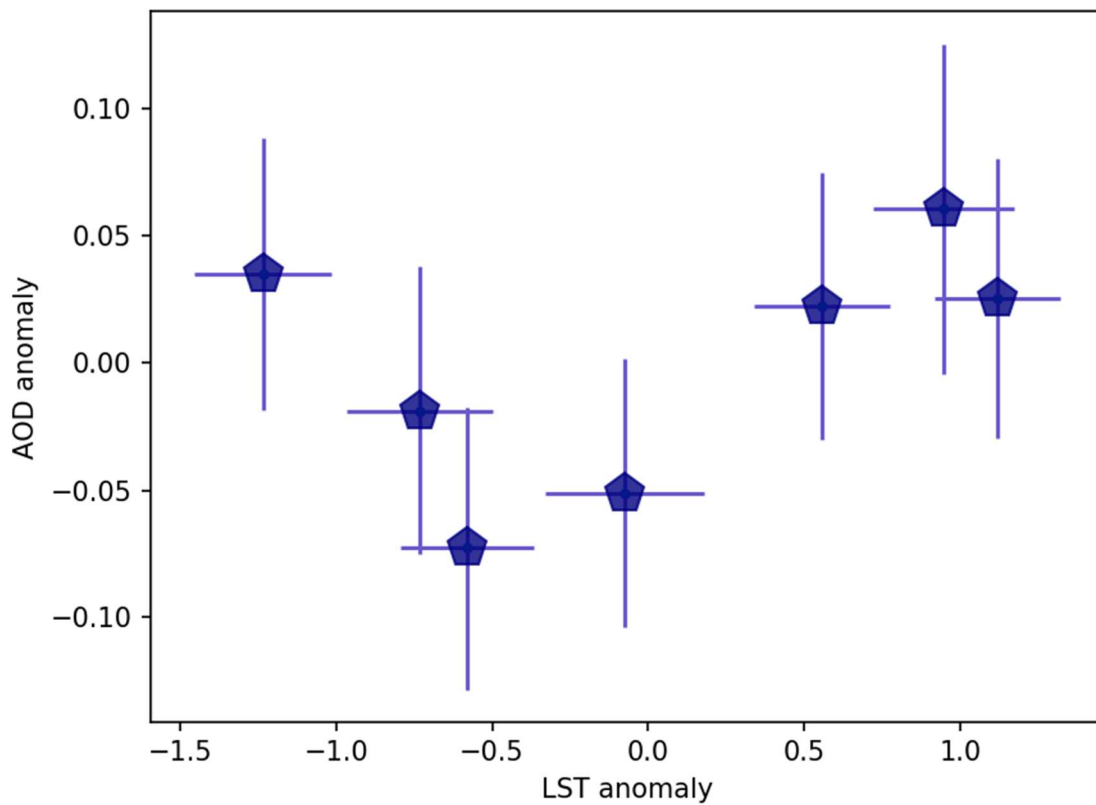


Figure S7. Summertime anomalies (JJA) of aerosol optical depth (AOD) vs. regional mean land surface temperature (LST) over mixed forests in the southeastern USA for the years 2005–2011. Pentagons represent averages over the whole domain. LST and AOD are from L3 AATSR. The error bars represent the uncertainty of the observations (one standard deviation).

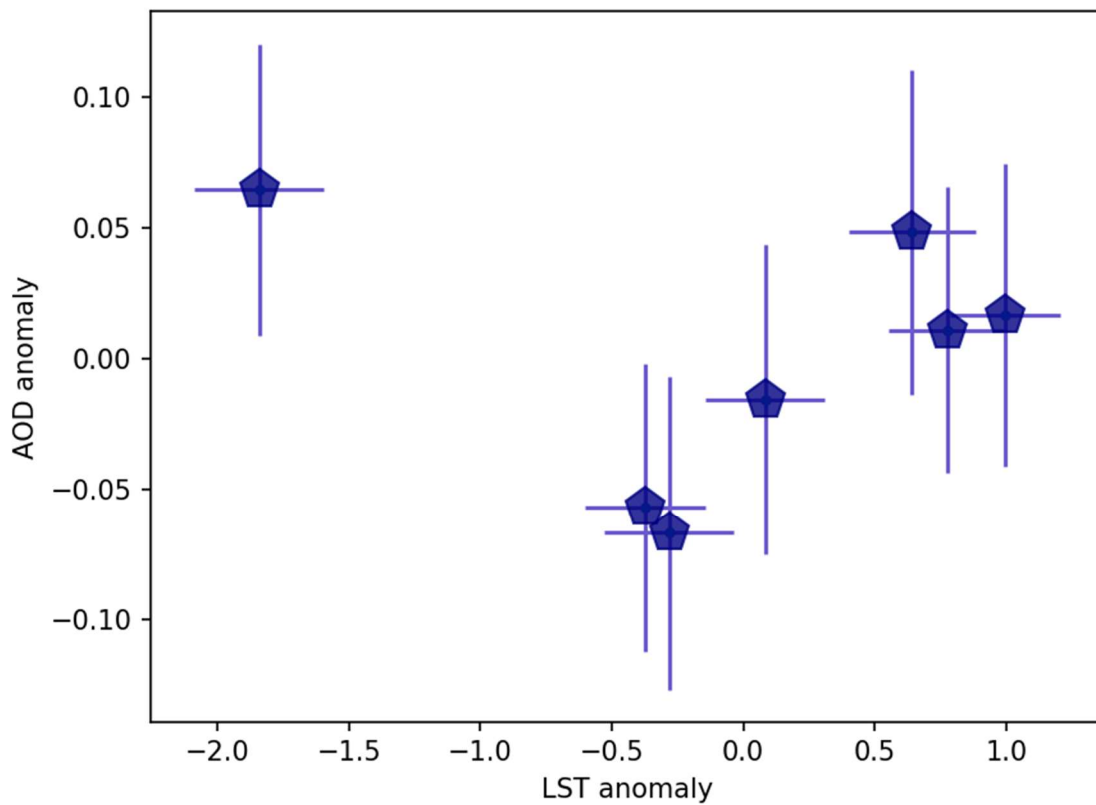


Figure S8. Summertime anomalies (JJA) of aerosol optical depth (AOD) vs. regional mean land surface temperature (LST) over woody savannas in the southeastern USA for the years 2005–2011. Pentagons represent averages over the whole domain. LST and AOD are from L3 AATSR. The error bars represent the uncertainty of the observations (one standard deviation).

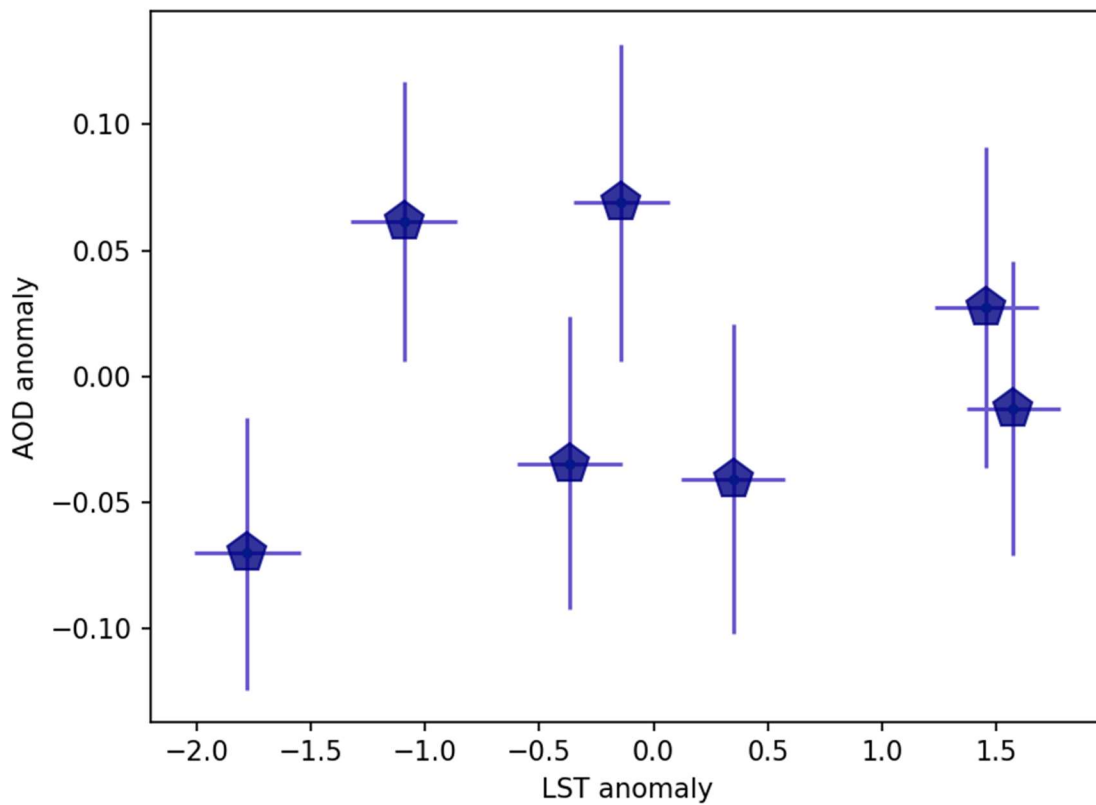


Figure S9. Summertime anomalies (JJA) of aerosol optical depth (AOD) vs. regional mean land surface temperature (LST) over cropland/natural mosaic in the southeastern USA for the years 2005–2011. Pentagons represent averages over the whole domain. LST and AOD are from L3 AATSR. The error bars represent the uncertainty of the observations (one standard deviation).

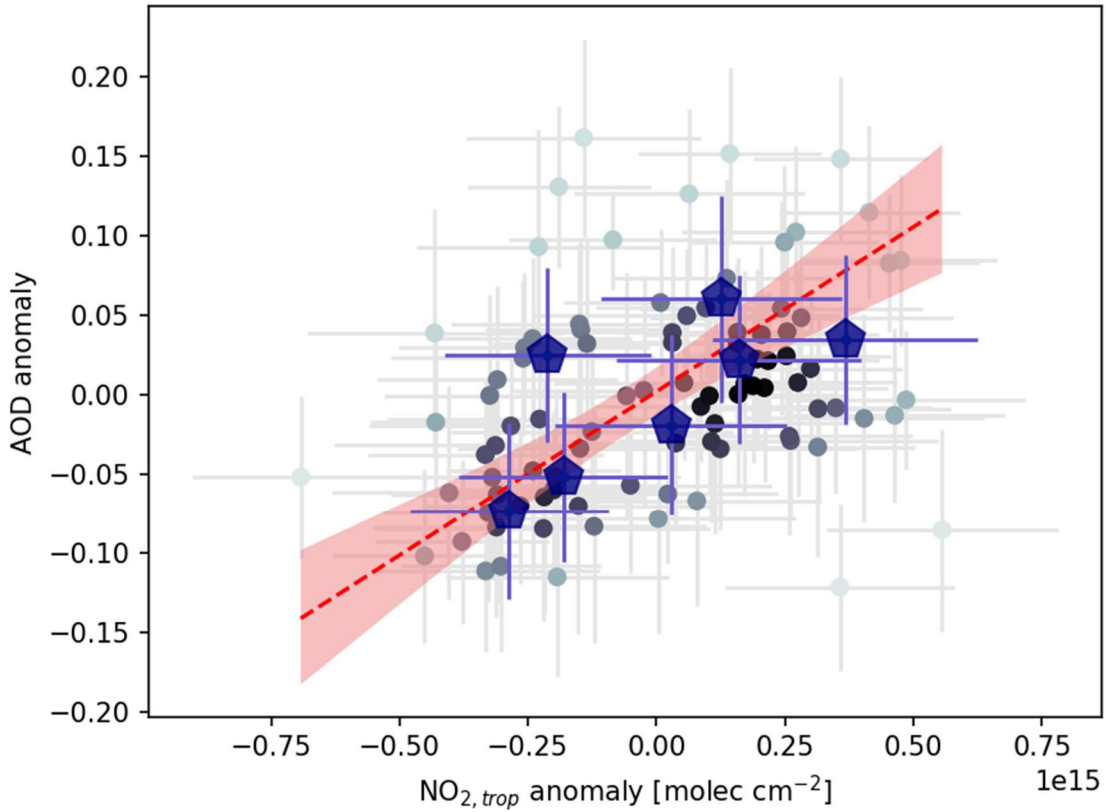


Figure S10. Summertime (JJA) anomalies of AOD vs. tropospheric NO_2 column densities over mixed forests in the southeastern USA for the years 2005–2011. Blue pentagons represent averages over the whole domain ($r = 0.70$) while the dots represent $1^\circ \times 1^\circ$ degree pixels within the domain. AOD is from L3 AATSR and tropospheric NO_2 from L3 OMI. The error bars represent the uncertainty of the observations (one standard deviation). The linear fit shown with the red dashed line is based on the individual data points ($AOD_{anom, MF} = 2.07e^{-16} (\pm 5.99e^{-17})NO_{2,trop,anom} + 0.002 (\pm 0.014)$), 91 observations, $r = 0.35$, 95 % confidence intervals given in the parenthesis). The red curtain represents the 95 % confidence interval for the linear fit. The color of the dots indicates the density of the overlapping data points: the darker the color, the more overlapping points there are.

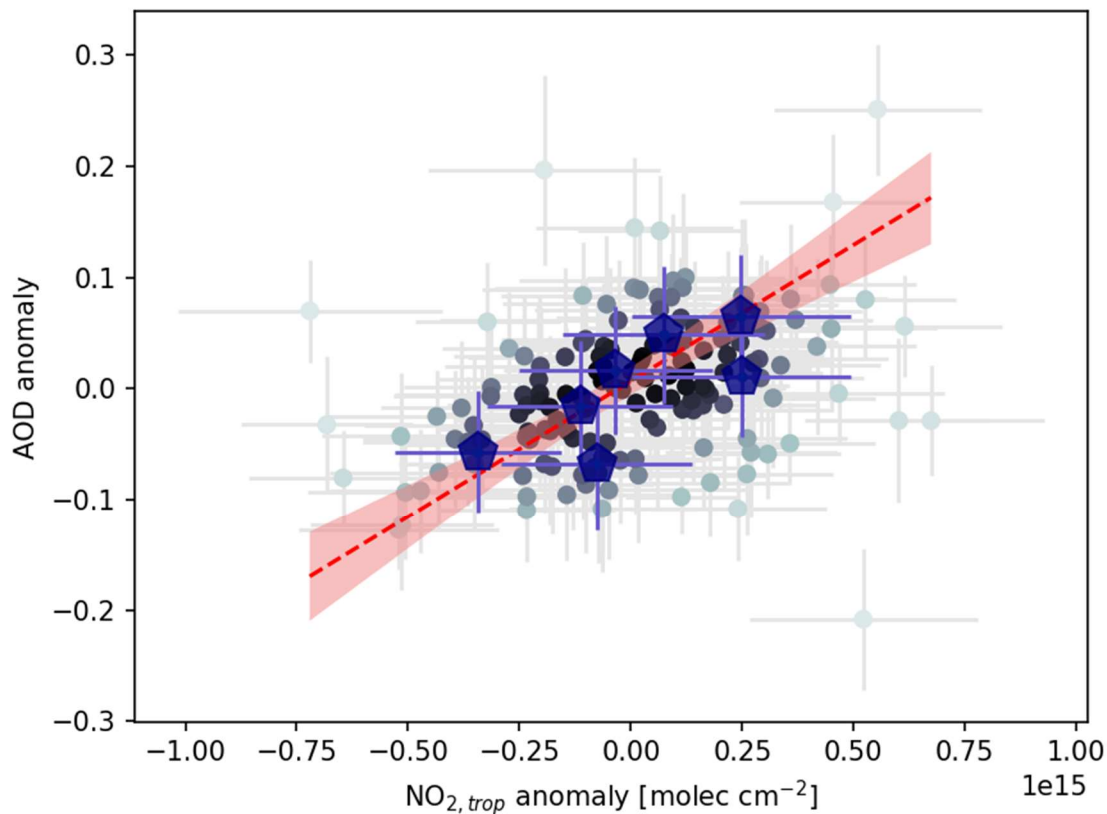


Figure S11. Summertime (JJA) anomalies of AOD vs. tropospheric NO_2 column densities over woody savannas in the southeastern USA for the years 2005–2011. Blue pentagons represent averages over the whole domain ($r = 0.76$) while the dots represent $1^\circ \times 1^\circ$ degree pixels within the domain. AOD is from L3 AATSR and tropospheric NO_2 from L3 OMI. The error bars represent the uncertainty of the observations (one standard deviation). The linear fit shown with the red dashed line is based on the individual data points ($AOD_{anom,WS} = 2.45e^{-16} (\pm 5.72e^{-1}) NO_{2,trop,anom} + 0.007 (\pm 0.013)$), 154 observations, $r = 0.35$, 95 % confidence intervals given in the parenthesis). The red curtain represents the 95 % confidence interval for the linear fit. The color of the dots indicates the density of the overlapping data points: the darker the color, the more overlapping points there are.

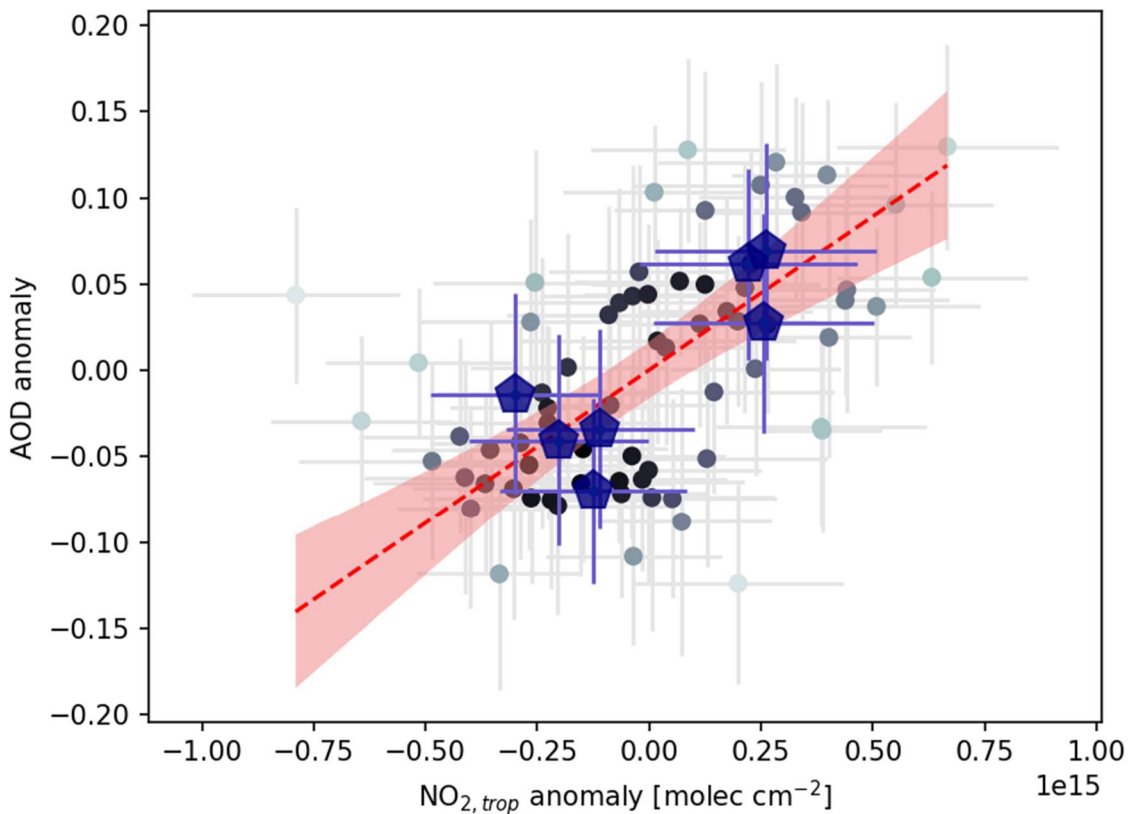


Figure S12. Summertime (JJA) anomalies of AOD vs. tropospheric NO_2 column densities over cropland/natural mosaic in the southeastern USA for the years 2005–2011. Blue pentagons represent averages over the whole domain ($r = 0.83$) while the dots represent $1^\circ \times 1^\circ$ degree pixels within the domain. AOD is from L3 AATSR and tropospheric NO_2 from L3 OMI. The error bars represent the uncertainty of the observations [one standard deviation]. The linear fit shown with the red dashed line is based on the individual data points ($AOD_{anom,CM} = 1.78e^{-16}(\pm 5.12e^{-17})NO_{2,trop,anom} + 0.000(\pm 0.015)$, 70 observations, $r = 0.50$, 95 % confidence intervals given in the parenthesis). The red curtain represents the 95 % confidence interval for the linear fit. The color of the dots indicates the density of the overlapping data points: the darker the color, the more overlapping points there are.

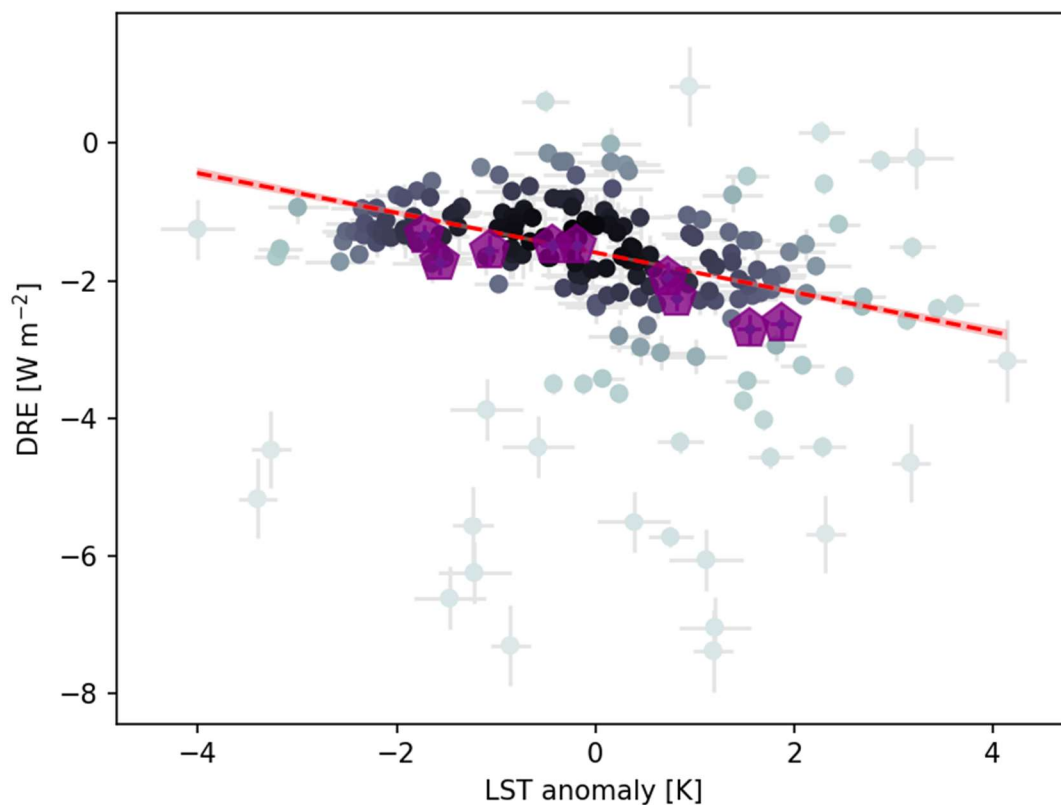


Figure S13: Biogenic aerosol direct radiative effect (DRE, based on the difference between the CONTROL and the noBIOSOA simulations) vs. LST anomaly for the summers (JJA) 2002-2010. Pentagons represent averages over the whole domain ($r = -0.89$) while the dots represent $1.9^\circ \times 1.9^\circ$ pixels within the domain. The dashed line represents the linear fit to the data ($DRE_{bio} = -0.29 (\pm 0.09)LST_{ano} - 1.59 (\pm 0.11)$, 198 points, $r = -0.19$, 95 % confidence intervals given in the parenthesis), the red curtain represents the 95 % confidence interval for the linear fit and the error bars represent the uncertainty caused by averaging.

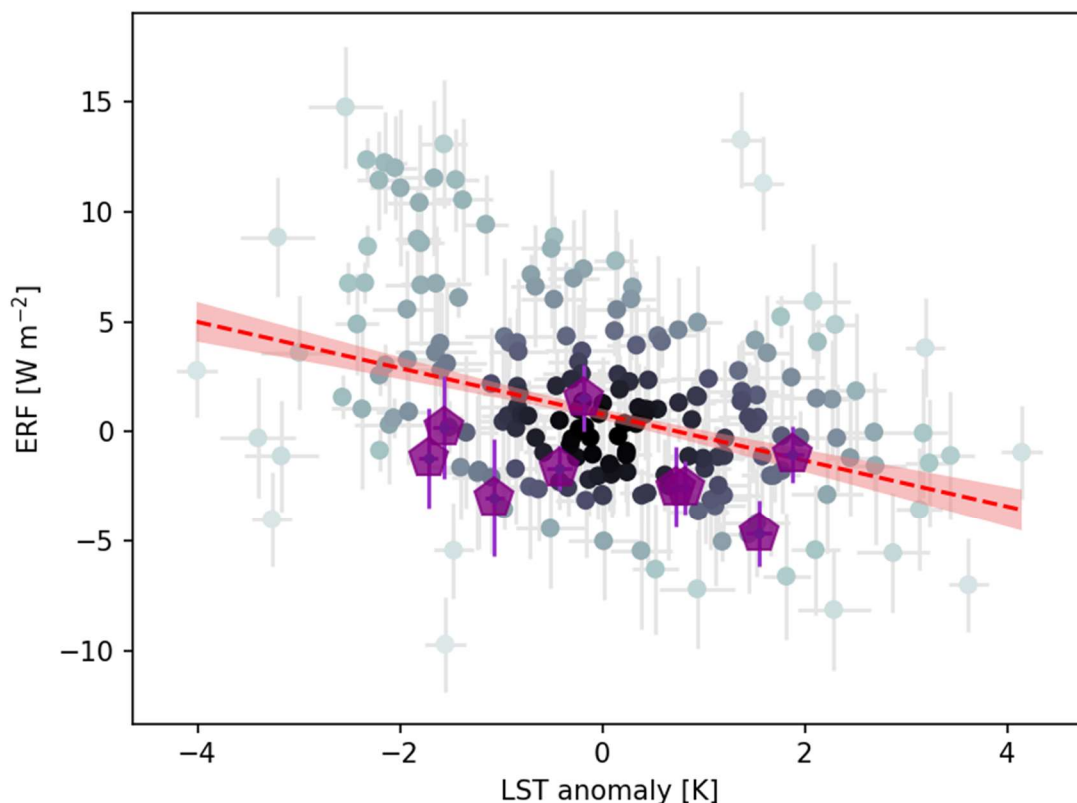


Figure S14: Effective radiative forcing caused by biogenic emissions (ERF, based on the difference between the CONTROL and the noBIOSOA simulations) vs. LST anomaly for the summers (JJA) 2002-2010. Pentagons represent averages over the whole domain ($r = -0.40$) while the dots represent $1.9^\circ \times 1.9^\circ$ pixels within the domain. The dashed line represents the linear fit to the data ($ERF_{bio} = -1.05(\pm 0.46)LST_{ano} + 0.80(\pm 0.53)$, 198 points, $r = -0.37$, 95 % confidence intervals given in the parenthesis), the red curtain represents the 95 % confidence interval for the linear fit and the error bars represent the uncertainty caused by averaging.

References

Alston, E. J., Sokolik, I. N. and Kalashnikova, O. V.: Characterization of atmospheric aerosol in the US Southeast from ground- and space-based measurements over the past decade, *Atmospheric Meas. Tech.*, 5(7), 1667–1682, doi:10.5194/amt-5-1667-2012, 2012.

Attwood, A. R., Washenfelder, R. A., Brock, C. A., Hu, W., Baumann, K., Campuzano-Jost, P., Day, D. A., Edgerton, E. S., Murphy, D. M., Palm, B. B., McComiskey, A., Wagner, N. L., de Sá, S. S., Ortega, A., Martin, S. T., Jimenez, J. L., Brown, S. S.: Trends in sulfate and organic aerosol mass in the Southeast U.S.: Impact on aerosol optical depth and radiative forcing, *Geophys. Res. Lett.*, 41, 7701–7709, doi:10.1002/2014GL061669, 2014.

Kolmonen, P., Sogacheva, L., Virtanen, T. H., de Leeuw, G. and Kulmala, M.: The ADV/ASV AATSR aerosol retrieval algorithm: current status and presentation of a full-mission AOD data set. *International Journal of Digital Earth*, 545-561, 2016.